Dielectric GaAs Antenna Ensuring an Efficient Broadband Coupling between an InAs Quantum Dot and a Gaussian Optical Beam

Mathieu Munsch, Nitin S. Malik, Emmanuel Dupuy, Adrien Delga, Joël Bleuse, Jean-Michel Gérard, and Julien Claudon*
CEA-CNRS-UJF Group, Nanophysique et Semiconducteurs, CEA, INAC, SP2M, F-38054 Grenoble, France

Niels Gregersen and Jesper Mørk
Department of Photonics Engineering, DTU Fotonik, Technical University of Denmark, Building 343, 2800 Kongens Lyngby, Denmark
(Received 20 September 2012; published 24 April 2013)

We introduce the photonic trumpet, a dielectric structure which ensures a nearly perfect coupling between an embedded quantum light source and a Gaussian free-space beam. A photonic trumpet exploits both the broadband spontaneous emission control provided by a single-mode photonic wire and the expansion of this mode within a conical taper. Numerical simulations highlight the performance and robustness of this concept. As a first application in the field of quantum optics, we report the realization of an ultrabright single-photon source. The device, a high aspect ratio GaAs photonic trumpet containing a few InAs quantum dots, demonstrates a first-lens external efficiency of 0.75 ± 0.1 and an external coupling efficiency to a Gaussian beam as high as 0.58 ± 0.08.

DOI: 10.1103/PhysRevLett.110.177402 PACS numbers: 78.67.Hc, 42.70.Qs, 78.55.Cr, 78.67.Pt

Optical waveguides that define a single-mode electromagnetic environment around a quantum light emitter are currently attracting a large amount of interest [1–6]. Compared to microcavities [7–9], their broad operation bandwidth considerably alleviates the fabrication constraints of bright sources of single photons and entangled photon pairs. Reversibly, these systems can also mediate strong nonlinear interactions between single photons, with direct applications to photonic quantum logic [10–14]. In most cases, the guided mode supported by such structures has to match a specific free-space mode, preferentially Gaussian. This property, which has attracted little attention so far, is desirable when feeding single photons into a single-mode optical fiber for quantum encrypted communications [15] or implementing an optical switch at the single-photon level [16]. The scalable interconnection of spin photon interfaces to realize a quantum network is also very demanding in terms of control over the far-field emission [17–20].

In this context, fiberlike photonic wires are simple dielectric waveguides with appealing performances [5,6,21,22]. For an emitter with a transverse optical dipole, they offer an efficient spontaneous emission (SE) control [23,24] (including polarization [25]) combined with low optical losses. A first step toward the control over their far-field emission has already been demonstrated [5,26] through the integration of a metal-dielectric mirror below the wire [27] and a needlelike tapering of its upper end [28]. Such a taper expands the guided mode outside the wire to obtain a directive far-field emission. However, as shown below, the emission remains poorly matched to a Gaussian free-space beam and is sensitive to minute geometrical details, thus compromising the device fabrication yield.

In this Letter, we solve these issues by expanding the guided mode inside a vertical conical taper. The resulting structure—a photonic trumpet—offers a unique combination of broad operation bandwidth, high extraction efficiency, and clean Gaussian far-field emission. In addition, the taper performance is very tolerant against geometrical changes, which alleviates fabrication constraints and ensures reproducible performances. After presenting theoretical design guidelines, we demonstrate the fabrication of such high-aspect ratio structures. As a first application in the field of quantum optics, we realize a very bright single-photon source with a first-lens external efficiency of 0.75 ± 0.1 and a record-high external coupling efficiency to a Gaussian beam of 0.58 ± 0.08.

We first consider an infinitely long vertical wire made of GaAs—a high index material ($n = 3.45$)—immersed in air or vacuum ($n_{\text{ext}} = 1$). The wire features a circular section of diameter d and embeds on its axis a single quantum dot (QD), with a free-space wavelength $\lambda = 950$ nm. The QD is modeled by a pointlike emitter with two transverse, orthogonal linear optical dipoles. We introduce β, the fraction of SE coupled to the family of fundamental guided modes (HE_{11}). It comprises an upward and a downward propagating mode, each one doubly polarization degenerated. The mode lateral confinement is quantified by the effective surface $S_{\text{eff}} = \iint n(x,y)^2|\mathbf{E}(x,y)|^2 dxdy / [n(0,0)^2|\mathbf{E}(0,0)|^2]$, where $\mathbf{E}$ is the electric field amplitude. As seen in Fig. 1(a), S_{eff} reaches a minimum value of $(0.18\lambda)^2$ for $d_1 = 240$ nm. For an on-axis emitter, β is then equal to 0.96 and exceeds 0.9 over a 250 nm broad operation bandwidth [23]. However, the tightly confined HE_{11} photons leaving a real, finite wire through a flat top facet are scattered to high angles into free space, which prevents the efficient collection of light with standard

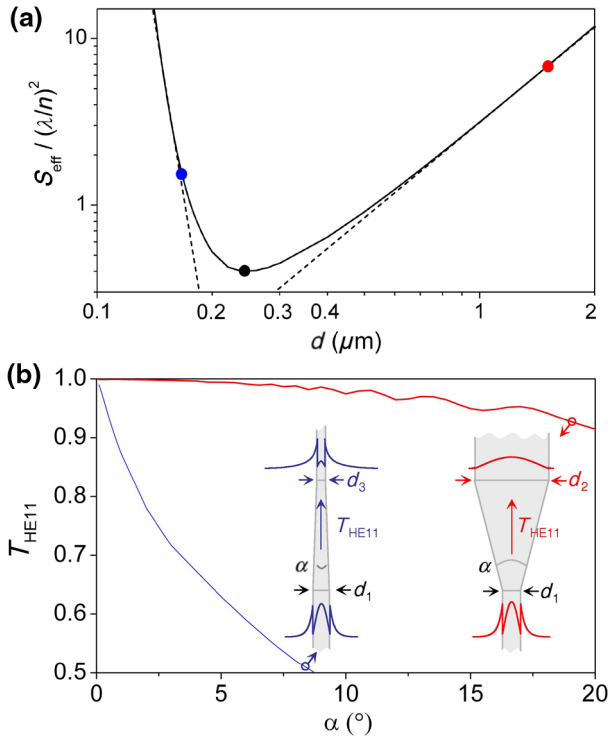

FIG. 1 (color online). Fundamental guided mode in a tapered wire. (a) Effective surface (S_{eff}) of the mode HE_{11} guided by a cylindrical wire of diameter d (double log scale, operation wavelength $\lambda = 950$ nm). The dashed lines are guides for the eye, indicating the slope of $\log(S_{\text{eff}})$ vs $(\log d)$ in the "small" and "large" diameter range. (b) Modal transmission of HE_{11} ($T_{HE_{11}}$), plotted against the tapering angle α for two representative tapers. For the photonic trumpet, d_2 is set to 1.5 μm; in the needle taper, $d_3 = 166$ nm is chosen to ensure the same collection of the mode using a NA = 0.75 lens. Typical electrical field profiles are also shown (amplitude of the discontinuous component). The dots appearing in (a) correspond to d_1, d_2, and d_3.

optics. To solve this issue, the mode size should be increased either through a decrease or increase in d, resulting, respectively, in needlelike and trumpetlike tapers [Fig. 1(a)].

To investigate the propagation of HE_{11} along a tapered section, we introduce the modal transmission $T_{HE_{11}}$. This quantity is plotted against the taper angle α for representative needle and trumpet linear tapers in Fig. 1(b). A photonic trumpet ensures a nearly perfect adiabatic expansion of HE_{11} for $\alpha < 5°$, leading to $T_{HE_{11}} > 0.994$. On the other hand, for the same angle range, the needle taper already suffers from significant nonadiabatic losses, which result in free-space emission before reaching the taper end. Qualitatively, the striking contrast between the two tapers can be understood by inspecting Fig. 1(a). For a needle taper S_{eff} scales as $d^{-5.5}$, whereas for the trumpet S_{eff} scales as $d^{1.9}$. Along the taper, the rate of change in diameter is governed by α. For a given α, a weaker dependence of S_{eff} on d thus implies slower changes in the mode profile during its propagation, which eases the adiabatic transformation of HE_{11}. In a trumpet with $\alpha > 5°$, HE_{11} experiences an increasing coupling to higher order guided modes. The propagation dynamics is then more complex, but $T_{HE_{11}}$ still exceeds 0.95 for α as large as 15°. Such a tolerance on α considerably alleviates the fabrication constraints.

We now discuss the performances of a $h = 12$ μm high trumpet taper emitting into a lens with a numerical aperture (NA) of 0.75, which corresponds to the experimental realization detailed in the second part of the Letter. Given the high value of $T_{HE_{11}}$, the far-field emission is essentially governed by the scattering of HE_{11} when it reaches the top facet. Since its diameter d_2 can be accurately controlled by a standard fabrication process, this ensures reproducible taper performances. To suppress the top facet reflectivity, we cover it with a dielectric layer having a $\lambda/4$ optical thickness and an index $n_{\text{ar}} = 1.99$, which is close to the optimal one ($\sqrt{n_{\text{ext}} n} = 1.86$). For $d_2 > 1.5$ μm, the facet reflectivity is then smaller than 10^{-2}. We consider two figures of merit for the taper: the total transmission T into the collection lens and the transmission T_g to a Gaussian beam, using the same lens. Figure 2(a) shows T and T_g plotted against α and the corresponding d_2. The taper reflectivity being negligible, T depends essentially on the divergence of the output beam, and exceeds 0.96 for $d_2 > 1.5$ μm. Regarding the coupling to a Gaussian beam, T_g increases with d_2 to reach an optimal $T_g = 0.97$ for $d_2 = 2.6$ μm. Above this diameter, which corresponds to $\alpha = 11.5°$, T_g undergoes a slight oscillating decrease due to the onset of mode conversion inside the taper. For

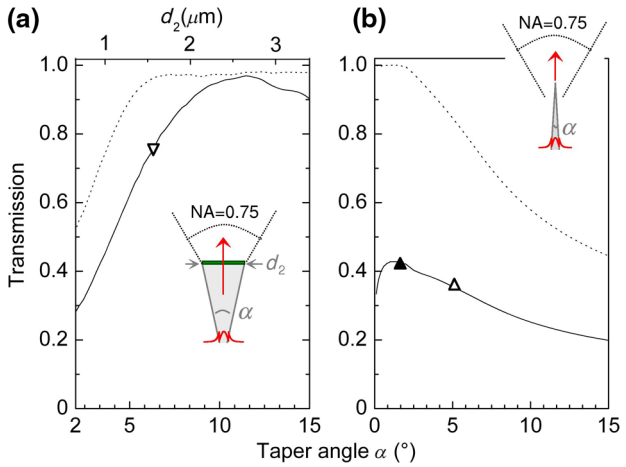

FIG. 2 (color online). Far-field emission. (a) Calculated total transmission T (dashed line) into a NA = 0.75 lens and transmission to a Gaussian beam T_g (solid line). The evaluation is conducted for a 12 μm high photonic trumpet with various taper angle α (and thus different top diameter d_2). The same quantities for a needle taper are shown in (b). Experimental realizations: needle tapers, upward open triangles (Ref. [5]); upward solid triangles (Ref. [22]); and photonic trumpet, downward open triangles (this work).

comparison, Fig. 2(b) shows T and T_g for a needle taper. Clearly, the maximum T_g in a trumpet exceeds by a factor >2.2 the value achievable with the sharpest needle taper ($T_g = 0.43$). This improvement essentially stems from the very favorable profile of HE_{11} when it exits the top facet of a trumpet [see inset in Fig. 1(b)].

Coming back to the emitter, symmetry imposes that half of the photons are emitted in the HE_{11} mode propagating downward. A mirror inserted below the trumpet reflects them back into the wire with an amplitude modal reflectivity r. Locating the emitter at an antinode of the resulting standing wave pattern enhances the SE rate into HE_{11} and optimizes the first lens external efficiency ϵ. For an emitter with a perfect radiative yield, $\epsilon = \frac{\beta(1+|r|)^2}{2(1+\beta|r|)}T$ [26]. The external coupling efficiency between the emitter and the Gaussian beam ϵ_g is obtained from the same formula, using T_g instead of T. As detailed in Ref. [27], a planar gold-silica mirror offers a modal reflectivity $|r| > 0.95$ for the wire diameters of interest. For an on-axis emitter $\beta = 0.96$, leading to $\epsilon_g = 0.95 \times T_g$. Considering the high value for T_g reached with a trumpet taper, this strategy offers a close to ideal coupling between a localized quantum emitter and a directive Gaussian beam. Noteworthy, thanks to the pronounced inhibition of the coupling to the nonguided modes, β is relatively robust against a misalignment between the emitter and the wire axis [23]. Thus, this broadband strategy is particularly relevant for self-assembled InAs QDs, which are fast and stable quantum light emitters but intrinsically suffer from spatial and spectral randomness [29]. Following Ref. [23], in a single-mode wire, one randomly located QD out of 15 experiences $\epsilon_g > 0.90 \times T_g$ and one QD out of 5 experiences $\epsilon_g > 0.80 \times T_g$.

In the following we demonstrate the high performance of photonic trumpets through the realization of an on-demand, ultrabright single-photon source. The device, shown in Fig. 3(b), is a 12 μm high cone with a tapering angle $\alpha = 6.5°$. Its top facet features a diameter $d_2 = 1.55$ μm and is covered by a Si_3N_4 antireflection coating ($n_{ar} = 1.99$, thickness: 115 nm). The bottom part of the trumpet presents a diameter in the 200–240 nm range, corresponding to the optimum field confinement. The structure is connected to a gold-silica planar mirror and embeds a few ($\sim 5 - 10$) InAs self-assembled QDs, located 110 nm above the mirror. The structure has been processed out of a planar sample grown by molecular beam epitaxy, using a top-down approach described in the Supplemental Material [30]. In particular, the trumpet is defined with a carefully optimized plasma etching, so as to obtain the right balance between physical sputtering and chemical etching. The scanning electron micrograph large view in Fig. 3(a) illustrates the reproducibility of the fabrication; the zooms in Figs. 3(b) and 3(c) show the excellent control over the trumpet geometry, notably the connection to the planar mirror. Despite

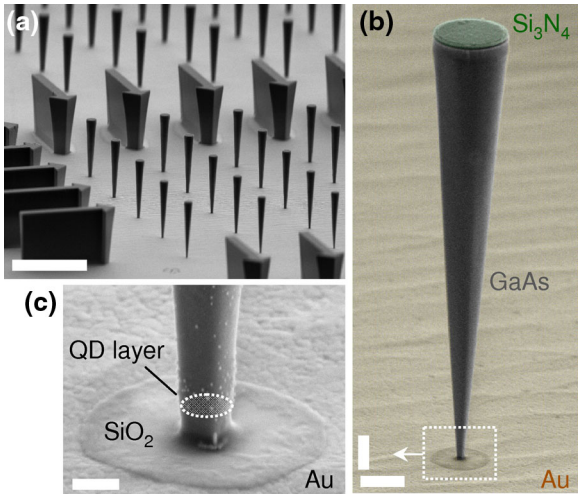

FIG. 3 (color online). Single-photon trumpets. (a) Scanning electron microscope view of a large field of devices, illustrating the reproducibility of the fabrication process. Scale bar: 15 μm. (b) Zoom on a representative device (false colors online); note the excellent control over the structure geometry. Vertical and horizontal scale bars: 1 μm. (c) Zoom on the connection between the trumpet and the integrated mirror. Scale bar: 200 nm.

their high-aspect ratio, these structures are robust enough to be manipulated in the lab without specific precaution. The final processing step, which involves wetting and dewetting by a liquid solution, constitutes in itself a stringent test for the structure resistance.

The source is operated at liquid helium temperature, using a microphotoluminescence (μPL) setup equipped with a commercial microscope objective (NA = 0.75). QD excitation is provided by a pulsed laser, tuned to the absorption continuum of the QD wetting layer, below the GaAs band gap. Figure 4(a) shows the spatial distribution of the QD emission in the top facet plane: it presents a Gaussian shape, which describes satisfyingly HE_{11} for this range of lateral confinement. The μPL spectrum features separated sharp lines, associated with QD excitonic transitions (Fig. 4(b)). In the following, we focus on three lines labeled 1, 2, and 3 ($\lambda = 902.5$ nm, 907.1 nm, 935.1 nm) associated with three different QDs. Their spectrally integrated intensities I_{int}, obtained from a fit to a Lorentzian line shape, are plotted against the pump power in Fig. 4(c). Considering the low power dependence of I_{int} and the measured transition decay time T_1, lines 1 and 3 are attributed to the recombination of an exciton and line 2 to the recombination of a biexciton.

In each case, single-photon emission is assessed with a measurement of the intensity autocorrelation function $g_2(\tau) = \langle I(t)I(t+\tau)\rangle/\langle I(t)\rangle^2$, where the brackets represent a time averaging. The measurement is performed under pulsed excitation, using a Hanbury Brown–Twiss setup which employs two silicon avalanche photodiodes (see the Supplemental Material [30]). The raw values of $g_2(0)$ for lines 1–3 are indicated in Fig. 4(c). They are

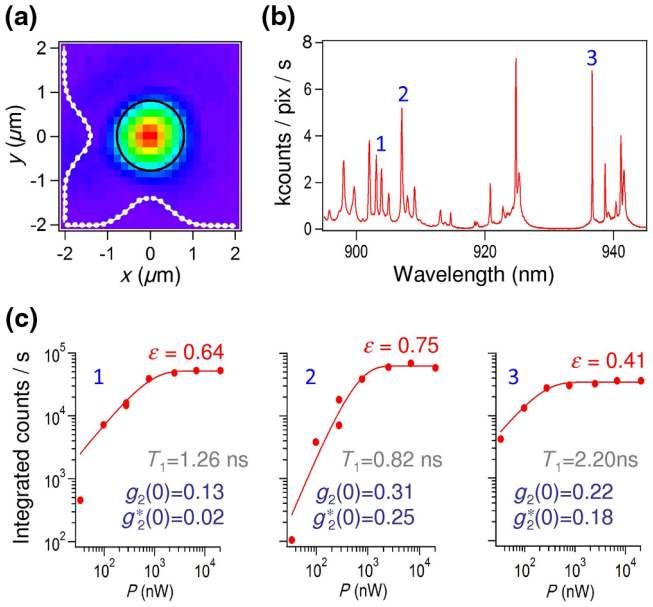

FIG. 4 (color online). Optical characterization. (a) Spatial distribution of the intensity in the top facet plane. At the location of the QD, only HE_{11} is guided by the structure and all the QDs contribute to the signal. Two diameter cuts and their fit to a Gaussian profile are also shown. The circle represents the facet circumference. (b) Microphotoluminescence spectrum, measured at $T = 5$ K for an excitation power $P = 20$ μW. (c) Spectrally integrated intensity of the lines 1, 2, and 3, extracted from a fit to a Lorentzian line shape, as a function of P. The solid lines are theory, assuming an excitonic emission (lines 1 and 3) and biexcitonic emission (line 2). For each transition, the luminescence decay time T_1, the raw and background-corrected intensity autocorrelation values $g_2(0)$ and $g_2^\star(0)$ are also shown.

smaller than 0.5, proving that the emission is dominated by the radiative recombination of a single electron-hole pair. Compared to our previous work [5], the higher dot density generates a sizeable luminescence background. Its contribution is removed in $g_2^\star(0)$, assuming statistical independence between the signal and a Poissonian background. In particular, line 1 exhibits $g_2^\star(0) = 0.02$, the signature of a pure single-photon emission.

The first lens external efficiency ϵ of the source was determined through careful calibration of the setup, conducted using a laser tuned to the QD emission wavelength as a reference (see the Supplemental Material [30]). The values that are given in the following include the two QD polarizations, and are corrected from residual multiphoton events. When driven to saturation, line 2 exhibits $\epsilon = 0.75 \pm 0.1$, placing our source among the brightest solid-state single-photon sources [5,31]. The small difference with the maximal theoretical value for the fabricated device ($\epsilon = 0.89$) is attributed to a nonoptimal lateral positioning of the QD and/or a residual fluctuation of its charge state. Furthermore, lines 1 and 3 are also very bright ($\epsilon = 0.61$ and 0.41), illustrating directly the broad operation bandwidth and tolerance with regard to the emitter's lateral position. Efficiencies in the 0.5–0.6 range were routinely obtained in other devices, further confirming the robustness of this approach.

The external coupling efficiency to a Gaussian beam can be derived from $\epsilon_g/\epsilon = T_g/T$. Using the calculated values $T = 0.96$ and $T_g = 0.75$ together with the measured $\epsilon = 0.75$, one obtains $\epsilon_g = 0.58 \pm 0.08$. This represents a major improvement over the state of the art: $\epsilon_g = 0.25$ for a QD-oxide aperture micropillar cavity [18], 0.30 for a QD-needlelike photonic wire [5], and 0.33 for a QD-etched micropillar [32] (in all cases, ϵ_g is derived from the experimental ϵ multiplied by the calculated mode matching to a Gaussian beam). In the future, T_g could be brought close to 1 by defining a top facet ~ 1 μm wider [Fig. 2(a)], either by increasing the taper angle or height. This would also lead to a very directive far-field emission, thus enabling the use of collection optics with a moderate numerical aperture. For example, a 12 μm high trumpet with $d_2 = 2.6$ μm ensures $T_g = 0.93$ into a lens with NA = 0.5.

In conclusion, photonic trumpets offer a unique combination of broad operation bandwidth, high extraction efficiency and Gaussian far-field emission. The expansion of HE_{11} inside a trumpet taper is also very tolerant against a change in the taper angle. This approach, that also offers a robust SE control, thus ensures reproducible performances. We have also successfully fabricated such high-aspect ratio structures and demonstrated an on-demand ultrabright single-photon source. Regarding advanced quantum light sources, the circular top facet is very convenient to add a top electrode [32,33], which is desirable to provide an electrical charge injection in the QD [34], or to tune its fine spectral properties with an electric field [35,36]. When required, an efficient polarization control could be implemented in a trumpet having an elliptical base [25]. Photonic trumpets thus feature key assets for the future developments of solid-state quantum optics, particularly when several detuned optical transitions are involved.

The authors acknowledge the support of the French Agence Nationale de la Recherche under grant WIFO. The sample fabrication has been performed in the Plateforme Technologique Amont and CEA Léti/DOPT/SIONA clean rooms.

Note added.—After submission of this work, a very bright single-photon source based on a QD inserted in a resonant micropillar cavity has been demonstrated [37]. The device, obtained with a carefully optimized fabrication process, combines a large external efficiency with a directive Gaussian far-field emission.

*julien.claudon@cea.fr

[1] E. Viasnoff-Schwoob, C. Weisbuch, H. Benisty, S. Olivier, S. Varoutsis, I. Robert-Philip, R. Houdré, and C. J. M. Smith, Phys. Rev. Lett. **95**, 183901 (2005).

[2] T. Lund-Hansen, S. Stobbe, B. Julsgaard, H. Thyrrestrup, T. Sünner, M. Kamp, A. Forchel, and P. Lodahl, Phys. Rev. Lett. **101**, 113903 (2008).

[3] Q. Quan, I. Bulu, and M. Lončar, Phys. Rev. A **80**, 011810 (2009).

[4] A. Akimov, A. Mukherjee, C. L. Yu, D. E. Chang, A. S. Zibrov, P. R. Hemmer, H. Park, and M. D. Lukin, Nature (London) **450**, 402 (2007).

[5] J. Claudon, J. Bleuse, N. S. Malik, M. Bazin, P. Jaffrennou, N. Gregersen, C. Sauvan, P. Lalanne, and J.-M. Gérard, Nat. Photonics **4**, 174 (2010).

[6] T. M. Babinec, B. M. Hausmann, M. Khan, Y. Zhang, J. R. Maze, P. R. Hemmer, and M. Lončar, Nat. Nanotechnol. **5**, 195 (2010).

[7] J. M. Gérard, Top. Appl. Phys. **90**, 269 (2003).

[8] K. J. Vahala, Nature (London) **424**, 839 (2003).

[9] J. P. Reithmaier, Semicond. Sci. Technol. **23**, 123001 (2008).

[10] D. E. Chang, A. S. Sørensen, E. A. Demler, and M. D. Lukin, Nat. Phys. **3**, 807 (2007).

[11] D. Roy, Phys. Rev. Lett. **106**, 053601 (2011).

[12] H. Zheng, D. J. Gauthier, and H. U. Baranger, Phys. Rev. Lett. **107**, 223601 (2011).

[13] P. Kolchin, R. F. Oulton, and X. Zhang, Phys. Rev. Lett. **106**, 113601 (2011).

[14] D. Valente, Y. Li, J. P. Poizat, J. M. Gérard, L. C. Kwek, M. F. Santos, and A. Auffèves, Phys. Rev. A **86**, 022333 (2012).

[15] N. Gisin, G. Ribordy, W. Tittel, and H. Zbinden, Rev. Mod. Phys. **74**, 145 (2002).

[16] V. Loo, C. Arnold, O. Gazzano, A. Lemaître, I. Sagnes, O. Krebs, P. Voisin, P. Senellart, and L. Lanco, Phys. Rev. Lett. **109**, 166806 (2012).

[17] H. J. Kimble, Nature (London) **453**, 1023 (2008).

[18] M. T. Rakher, N. Stoltz, L. A. Coldren, P. M. Petroff, and D. Bouwmeester, Phys. Rev. Lett. **102**, 097403 (2009).

[19] W. B. Gao, P. Fallahi, E. Togan, J. Miguel-Sanchez, and A. Imamoglu, Nature (London) **491**, 426 (2012).

[20] K. D. Greve, L. Yu, P. L. McMahon, J. S. Pelc, C. M. Natarajan, N. Y. Kim, E. Abe, S. Maier, C. Schneider, M. Kamp, S. Höfling, R. H. Hadfield, A. Forchel, M. M. Fejer, and Y. Yamamoto, Nature (London) **491**, 421 (2012).

[21] J. Heinrich, A. Huggenberger, T. Heindel, S. Reitzenstein, S. Höfling, L. Worschech, and A. Forchel, Appl. Phys. Lett. **96**, 211117 (2010).

[22] M. E. Reimer, G. Bulgarini, N. Akopian, M. Hocevar, M. B. Bavinck, M. A. Verheijen, E. P. Bakkers, L. P. Kouwenhoven, and V. Zwiller, Nat. Commun. **3**, 737 (2012).

[23] J. Bleuse, J. Claudon, M. Creasey, N. S. Malik, J.-M. Gérard, I. Maksymov, J.-P. Hugonin, and P. Lalanne, Phys. Rev. Lett. **106**, 103601 (2011).

[24] G. Bulgarini, M. E. Reimer, T. Zehender, M. Hocevar, E. P. A. M. Bakkers, L. P. Kouwenhoven, and V. Zwiller, Appl. Phys. Lett. **100**, 121106 (2012).

[25] M. Munsch, J. Claudon, J. Bleuse, N. S. Malik, E. Dupuy, J.-M. Gérard, Y. Chen, N. Gregersen, and J. Mørk, Phys. Rev. Lett. **108**, 077405 (2012).

[26] I. Friedler, C. Sauvan, J. P. Hugonin, P. Lalanne, J. Claudon, and J. M. Gérard, Opt. Express **17**, 2095 (2009).

[27] I. Friedler, P. Lalanne, J. P. Hugonin, J. Claudon, J. M. Gérard, A. Beveratos, and I. Robert-Philip, Opt. Lett. **33**, 2635 (2008).

[28] N. Gregersen, T. R. Nielsen, J. Claudon, J. M. Gérard, and J. Mørk, Opt. Lett. **33**, 1693 (2008).

[29] A. Shields, Nat. Photonics **1**, 215 (2007).

[30] See Supplemental Material at http://link.aps.org/supplemental/10.1103/PhysRevLett.110.177402 for technical details on the simulations, the optical setup, and the measurement of the external efficiency.

[31] K. G. Lee, X. W. Chen, H. Eghlidi, P. Kukura, R. Lettow, A. Renn, V. Sandoghdar, and S. Götzinger, Nat. Photonics **5**, 166 (2011).

[32] T. Heindel, C. Schneider, M. Lermer, S. H. Kwon, T. Braun, S. Reitzenstein, S. Höfling, M. Kamp, and A. Forchel, Appl. Phys. Lett. **96**, 011107 (2010).

[33] N. Gregersen, T. R. Nielsen, J. Mørk, J. Claudon, and J.-M. Gérard, Opt. Express **18**, 21204 (2010).

[34] Z. Yuan, B. Kardynal, R. Stevenson, A. Shields, C. Lobo, K. Cooper, N. Beattie, D. Ritchie, and M. Pepper, Science **295**, 102 (2002).

[35] J. J. Finley, M. Sabathil, P. Vogl, G. Abstreiter, R. Oulton, A. I. Tartakovskii, D. J. Mowbray, M. S. Skolnick, S. L. Liew, A. G. Cullis, and M. Hopkinson, Phys. Rev. B **70**, 201308(R) (2004).

[36] A. J. Bennett, M. A. Pooley, R. M. Stevenson, M. B. Ward, R. B. Patel, A. B. de la Giroday, N. Sköld, I. Farrer, C. A. Nicoll, D. A. Ritchie, and A. J. Shields, Nat. Phys. **6**, 947 (2010).

[37] O. Gazzano, S. M. de Vasconcellos, C. Arnold, A. Nowak, E. Galopin, I. Sagnes, L. Lanco, A. Lemaître, and P. Senellart, Nat. Commun. **4**, 1425 (2013).